

Angular momentum preserving schemes for compressible Euler equations

Elena Gaburro^{*a,e}, Bruno Després^{b,c}, Stéphane Del Pino^d, Michael Dumbser^a

^aDepartment of Civil, Environmental and Mechanical Engineering, University of Trento, Via Mesiano, 77 - 38123 Trento, Italy.

^bUPMC Univ paris 06, UMR 7598, Laboratoire J.-L. Lions, F-75005 Paris, France

^cInstitut Universitaire de France

^dCEA, DAM, DIF, F-91297 Arpajon, France

^eDepartment of Mathematics, University of Trento, Via Sommarive, 14 - 38123 Trento, Italy

Abstract

In this paper we investigate the conservation of the *angular momentum* for the Euler equations of compressible gas dynamics. We propose a method able to discretize, besides to the standard quantities, *i.e.* mass, inertial momentum and energy, the angular momentum, and we study the positive effects of considering this adjoint physical variable on the entire system. We propose both a master-slave approach and some coupled approaches in order to exploit the benefit provided by explicitly considering the conservation law regarding the angular momentum (redundant from the analytical point of view, but extremely interesting from numerical purposes, especially for *vortical flows*). Simple test cases open important issues in terms of imposition of appropriate boundary conditions and proper definition of the angular momentum, in particular when the center of rotation is not known *a priori*. For this last reason, we introduce a *detector* able to reconstruct locally the centers of rotation or of explosion of a generic problem given its velocity field and its pressure field. This detector provides supplementary information over the studied system and can also be applied for a convenient definition of the angular momentum. A new Kidder solution with rotation is derived in cylindrical coordinates.

Key words: Euler equations of compressible gas dynamics, angular momentum preserving scheme, rotation and explosion problems, hyperbolic conservation laws, vortical flows, center-detector.

1. Introduction

This work intends to contribute to a long lasting debate in computational fluid dynamics which is the enhancement of the accuracy of compressible fluid solvers for vortical flows. In the literature one can distinguish two main approaches: the first one based on vorticity and the second one based on angular momentum. For a general review on vorticity in standard finite volume schemes we refer to Roe [19] and for the case of Lagrangian methods we mention the seminal work of Dukowicz and Meltz in [11]. Other references are in the recent contribution [18]. Concerning angular momentum, we cite the recent results of Després and Labourasse [10] where the angular momentum is added to the system (with an initial approach similar to the one of this paper) and treated with a partial Discontinuous Galerkin discretization. In particular, they show that considering the angular momentum enhances the accuracy of implosion calculations and minimizes the mesh imprint. In this work, we address angular momentum preservation in the framework of *Eulerian and Arbitrary Lagrangian Eulerian methods* [3]: these methods are characterized by a moving computational domain whose velocity can be set to zero to reproduce the Eulerian case, or can be chosen as

*Corresponding author

Email addresses: elena.gaburro@unitn.it (Elena Gaburro*), despres@ann.jussieu.fr (Bruno Després), stephane.delpino@cea.fr (Stéphane Del Pino), michael.dumbser@unitn.it (Michael Dumbser)

Preprint submitted to *Computers and Fluids*

February 23, 2018

soon as possible equal to the local fluid velocity, as it is in the pure Lagrangian context, or slightly modified in an arbitrary way in order to maintain a better quality of the mesh.

There exists a wide range of applications for which the *conservation of angular momentum* is an issue. A first example is fluid simulations of the atmosphere around the earth for which the angular momentum of the atmosphere may interact with the angular momentum of the planet itself, we refer to [17] for an early work on the theme. A completely different physical problem is rotation of MHD flows in Tokamaks for which angular preservation is clearly a fundamental issue. It is addressed in the context of MHD solvers, either full MHD or reduced MHD, and a general review can be found in [13]. We notice that finite volume techniques are rarely used in the Tokamaks community. On the other hand Godunov solvers are widely used for astrophysical flows, and angular momentum is a key feature for an accurate numerical treatment of rotation of stars and planets: many works are devoted to this issue on Cartesian fixed grids and we quote only on few of them such as [16, 20]. In this context, Käppeli and Mishra have recently proposed a Godunov scheme in the Eulerian frame to address the issue of angular momentum conservation [14]. A last case regards the chemical reactions into the combustion chamber of engines [1]: in this situation the initial stage of turbulent flows is dominated by strong vortexes inside the flow and so its study could be improved taking into account the angular momentum.

What we propose here is to *exploit* in various ways the *redundant conservation law* that can be written for the angular momentum. Indeed, our study is based on considering an augmented Euler system of equations where we take into account both the inertial momentum conservation law as well as the angular momentum conservation law. Then we consider various formulations of this augmented system that can be easily handled by our code, which is able to discretize arbitrary hyperbolic systems written in the form

$$\frac{\partial \mathbf{Q}}{\partial t} + \nabla \cdot \mathbf{F}(\mathbf{Q}, \mathbf{x}) = \mathbf{S}(\mathbf{Q}), \quad \mathbf{x} \in \Omega(t) \subset \mathbb{R}^2, \quad \mathbf{Q}(t, \mathbf{x}) \in \mathbb{R}^\nu,$$

where \mathbf{Q} is the vector of the conserved quantities and $\mathbf{F}(\mathbf{Q}, \mathbf{x})$ a non linear flux tensor that depends both on \mathbf{Q} and on the position \mathbf{x} . In particular, three formulations will be presented in this paper, the master-slave approach, the global-coupling and the local-coupling. In the master-slave approach we propose a straightforward discretization of the augmented system, where the angular momentum will have no influence on the other conserved variables. In the global-coupling the angular momentum is strongly coupled with the entire system: in this case we will assume the *a priori* knowledge of a fixed center of rotation. Finally, for the local-coupling we will explore a solution in which the rotation center varies locally. In these three approaches $\nu = 5$ whereas for the initial Euler system $\nu = 4$.

The *validation* of the different algorithms will be performed with three different types of test problems. The first one is standard and is used to compare the results for the three approaches (master-slave approach, global-coupling and local-coupling). It is a solid body rotation of a gas with constant density. Density and velocity have been chosen in such a way that also the angular momentum is constant. As computational domain we consider a ring centered in the origin with radius $r \in [1, 2]$ and the initial condition, that corresponds also to the stationary analytical solution, is the following

$$\rho = 1, \quad \mathbf{u} = \left(\frac{-y}{x^2 + y^2}, \frac{x}{x^2 + y^2} \right), \quad p = -\frac{1}{2(x^2 + y^2)} + 1, \quad w = 1. \quad (1)$$

In Table 1 with this test, we illustrate the interest of solving the angular momentum within an augmented system. The second type of test is made of variants of the first one, to illustrate specific features of the different methods. The third test problem is a generalization of the Kidder test problem [5] which is emblematic of strong implosion in stars or inertial confinement devices. In our study we extend the physics considered in the standard Kidder problem by adding non zero angular velocity. To our knowledge, this new analytical solution in cylindrical coordinates which combines compression and rotation is original with respect to the literature.

The paper is organized as follows. First in Section 2, we introduce the augmented system of equations. The fundamental principles of a Finite Volume method are provided in Section 3. In Section 4 we introduce

Table 1: In the central column (*without Angular Momentum Conservation* – without AMC) we report the error in L_2 norm between the analytical value of the angular momentum and the one obtained at later times by computing *a posteriori* $w = \mathbf{u} \wedge (\mathbf{x} - \mathbf{x}_c)$, by solving a system of size $\nu = 4$. The errors reported in the right column (*with AMC*) are obtained with the master-slave approach (see Section 4), by solving an augmented system of size $\nu = 5$. We have employed a mesh of 1600 elements and both a method of order 1 and 2. This simple test proves that post-processing may generate important errors with respect to direct full computation of an augmented system.

time	without AMC ($\nu = 4$)		with AMC ($\nu = 5$, master-slave)	
	order 1	order 2	order 1	order 2
1	3.2	5.1E-3	2.6E-16	1.6E-16
5	7.2	3.0E-2	1.0E-15	8.2E-16
10	9.4	5.3E-2	2.1E-15	1.7E-15
20	-	1.0E-1	3.7e-15	3.2E-15

the master-slave formulation. Section 5 is devoted to the global-coupling algorithm. The principles of a center-detector are introduced in Section 6. Next, Section 7 is devoted to the local-coupling method. The coupling with some elementary ALE techniques is investigated in Section 8. In Section 9 we study a modified Kidder problem with rotation. In Section 10 we conclude giving an outlook on future extension of our research investigations. Some details of the derivation of the Kidder solution with rotation are in the Appendix A.

2. Augmented Euler equations

Let us recall the standard Euler equations of compressible gas dynamics in two dimensions of space which represent a strictly hyperbolic system

$$\begin{cases} \partial_t \rho + \nabla \cdot (\rho \mathbf{u}) = 0, \\ \partial_t (\rho \mathbf{u}) + \nabla \cdot (\rho \mathbf{u} \otimes \mathbf{u}) + \nabla p = \mathbf{0}, \\ \partial_t (\rho e) + \nabla \cdot (\rho \mathbf{u} e + p \mathbf{u}) = 0. \end{cases} \quad (2)$$

Here ρ is the density, $\mathbf{u} = (u_1, u_2)$ is the velocity, e is the total energy density and p the pressure. For a perfect gas one has

$$p = (\gamma - 1) \left(\rho e - \frac{1}{2} \rho \|\mathbf{u}\|^2 \right), \quad \gamma = \frac{c_p}{c_v} > 1, \quad (3)$$

where γ is the ratio between heats at constant pressure and volume, which is taken to be constant. In particular, we underline that the system states $\nu = 4$ conservation laws: one for the mass, two for the inertial momentum and the last for the energy. In any direction defined by the unit vector \mathbf{n} , (2) admits four eigenvalues: $u_n - c, u_n, u_n + c, u_n$, where c denotes the sound speed $c = \sqrt{\gamma p / \rho}$ and $u_n = \mathbf{u} \cdot \mathbf{n}$. From now on, for the sake of clarity, we detail everything in $2D$, but most of the ideas are general and can be easily extended to $3D$.

By choosing arbitrarily a special center point $\mathbf{x}_c = (x_c, y_c)$ the *angular momentum* can be defined as

$$w = \mathbf{u} \wedge (\mathbf{x} - \mathbf{x}_c), \quad \text{where } \wedge \text{ denotes the vector product.} \quad (4)$$

Note that $\mathbf{x}_c = \mathbf{0}$ is a possible choice and it is adopted when the center of rotation of the studied system is unique and known for any time. For the other cases we will describe a technique to determine it. Straightaway, a *redundant conservation law* for the angular momentum can be easily derived from the equations of the inertial momentum, by computing

$$(x - x_c) \left(\partial_t (\rho u_1) + \partial_x (\rho u_1^2 + p) + \partial_y (\rho u_1 u_2) \right) - (y - y_c) \left(\partial_t (\rho u_2) + \partial_x (\rho u_1 u_2) + \partial_y (\rho u_2^2 + p) \right), \quad (5)$$

from which we obtain

$$\partial_t(\rho w) + \nabla \cdot (\rho \mathbf{u} w + p(\mathbf{x} - \mathbf{x}_c)^\perp) = 0. \quad (6)$$

It is clear that, from an analytical point of view, this equation does not add any supplementary information to the system, since it is directly derived from the other ones. But from a numerical point of view it provides extra information in particular in the case of rotating systems.

Thus one can define the augmented 2D Euler system as

$$\begin{cases} \partial_t \rho + \nabla \cdot (\rho \mathbf{u}) = 0 \\ \partial_t(\rho \mathbf{u}) + \nabla \cdot (\rho \mathbf{u} \otimes \mathbf{u}) + \nabla p = 0 \\ \partial_t(\rho e) + \nabla \cdot (\rho \mathbf{u} e + p \mathbf{u}) = 0 \\ \partial_t(\rho w) + \nabla \cdot (\rho w \mathbf{u} + p(\mathbf{x} - \mathbf{x}_c)^\perp) = 0. \end{cases} \quad (7)$$

The system is still hyperbolic with an extra eigenvalue equal to u_n .

In Sections 4, 5 and 7 we will reformulate this system in order to obtain numerical methods with different characteristics. All of these will be automatically discretized thanks to our general Arbitrary Lagrangian Eulerian (ALE) PDE solver which is briefly described in the next section.

3. Numerical method

For all the test cases presented in this article we have employed an up to second order accurate direct cell-centered ALE scheme on unstructured polygonal grids (the order is specified for each employed approach). Lagrangian remesh and remap ALE schemes are very popular and some recent works on that topic for compressible flows can be found in [4]. In contrast to indirect ALE schemes (purely Lagrangian phase, remesh and subsequent remap phase) there are the so-called *direct ALE schemes*, where the local rezoning is performed before the computation of the numerical fluxes, hence changing directly the chosen mesh velocity of the ALE approach, see for example [6, 7, 8] for recent works in that direction based on high order ADER-WENO schemes.

Our ALE scheme is based directly on a space-time conservation formulation of the governing PDE system, hence is a direct ALE scheme. The algorithm can deal with any two-dimensional nonlinear hyperbolic system of conservations laws that can be cast in the following general form

$$\frac{\partial \mathbf{Q}}{\partial t} + \nabla \cdot \mathbf{F}(\mathbf{Q}, \mathbf{x}) = \mathbf{S}(\mathbf{Q}), \quad \mathbf{x} \in \Omega(t) \subset \mathbb{R}^2, \quad \mathbf{Q}(t, \mathbf{x}) \in \mathbb{R}^v, \quad (8)$$

where $\mathbf{x} = (x, y)$ is the spatial position vector, t represents the time, $\mathbf{Q} = (q_1, q_2, \dots, q_v)$ is the vector of conserved variables, $\mathbf{F}(\mathbf{Q}, \mathbf{x}) = (\mathbf{f}(\mathbf{Q}, \mathbf{x}), \mathbf{g}(\mathbf{Q}, \mathbf{x}))$ is the non linear flux tensor, and $\mathbf{S}(\mathbf{Q})$ represents a non linear algebraic source term. To discretize the moving domain, we consider an unstructured mesh \mathcal{T}_Ω^n with a total number N_E of polygonal elements T_i^n (the *spatial control volumes*) that covers the computational domain $\Omega(\mathbf{x}, t^n) = \Omega^n$ at time t^n . At each time step the new position of all the nodes is recomputed according to a prescribed velocity and the space-time control volumes $C_i^n = T_i(t) \times [t^n, t^{n+1}]$ are obtained by connecting via straight line segments each vertex of the element T_i^n with the corresponding vertex of T_i^{n+1} .

Then, as proposed in [7], the governing PDE (8) has been rewritten in a space-time divergence form as

$$\tilde{\nabla} \cdot \tilde{\mathbf{F}} = \mathbf{S}, \quad (9)$$

with

$$\tilde{\nabla} = (\partial_x, \partial_y, \partial_t)^T, \quad \tilde{\mathbf{F}} = (\mathbf{F}, \mathbf{Q}) = (\mathbf{f}, \mathbf{g}, \mathbf{Q}), \quad (10)$$

and it is then integrated over each space-time control volume

$$\int_{t^n}^{t^{n+1}} \int_{T_i(t)} \tilde{\nabla} \cdot \tilde{\mathbf{F}} \, dx dt = \int_{t^n}^{t^{n+1}} \int_{T_i(t)} \mathbf{S} \, dx dt. \quad (11)$$

Application of the Gauss theorem on the left-hand side, and integration over each lateral surface of the C_i^n gives us the final one-step scheme

$$|T_i^{n+1}| \mathbf{Q}_i^{n+1} = |T_i^n| \mathbf{Q}_i^n - \sum_j \int_0^1 \int_0^1 |\partial C_{ij}^n| \tilde{\mathbf{F}}_{ij} \cdot \tilde{\mathbf{n}}_{ij} d\chi d\tau + \int_{t^n}^{t^{n+1}} \int_{T_i(t)} \mathbf{S}(\mathbf{q}_h) dx dt, \quad (12)$$

where the discontinuity of the solution at the space–time surface is resolved by an ALE numerical flux function $\tilde{\mathbf{F}}_{ij} \cdot \tilde{\mathbf{n}}_{ij}$, which computes the flux between two neighbors across the intermediate space–time lateral surface. In particular, we are going to use the Rusanov flux, so the only requirement in order to apply our general scheme is the knowledge of the entire set of the eigenvalues of the system. Second order of accuracy in space and time is obtained by using a MUSCL-Hancock strategy [21], together with a Barth and Jespersen slope limiter [2].

For every further detail on the scheme we refer to [12] and the reference there in. We do not detail here the numerical scheme because it is out of the scope of this work where we would like to concentrate on the equation formulation. Similar results could be obtained with classical finite volume schemes able to deal with general hyperbolic equations. However, we would like to underline that the ALE context allows us to first employ a zero velocity mesh in order to investigate what happens in the Eulerian framework; we will switch to a moving domain in Section 8.

4. Master-slave approach

The first method we propose consists simply in discretizing (7) by setting

$$\mathbf{Q} := \begin{pmatrix} \rho \\ \rho \mathbf{u} \\ \rho e \\ \rho w \end{pmatrix} \quad \text{and} \quad \mathbf{F}(\mathbf{Q}, \mathbf{x}) := \begin{pmatrix} \rho \mathbf{u} \\ \rho \mathbf{u} \otimes \mathbf{u} + \mathbf{I} p \\ \rho \mathbf{u} e + p \mathbf{u} \\ \rho w \mathbf{u} + p(\mathbf{x} - \mathbf{x}_c)^\perp \end{pmatrix}$$

in (8) and use our general code. We refer to the fifth equation as slave because the Euler equations are solved independently, then angular momentum equation is computed *a posteriori*. This is regrettable because the benefits of angular momentum preservation cannot be seen by the other physical variables. However, by construction we automatically obtain the conservation in L_1 norm of w as adjoint variable. See Table 2 for some numerical results.

We would like to underline that the value assumed by w evolved through its conservation law may be different from the exact one and from the one computed *a posteriori* as $\mathbf{u} \wedge (\mathbf{x} - \mathbf{x}_c)$: indeed the evolution of \mathbf{u} and w are not linked in the master-slave formulation. For this reason the exact conservation of the total angular momentum does not imply directly an improvement on the final results. So, to measure the impact of our modified methods on the simulations we consider the following quantities

$$\|w - w_0\|_{L_2} = \sqrt{\sum_{i=1}^{N_E} |T_i| (w_i - w_{0,i})^2}, \quad \|\mathbf{u} - \mathbf{u}_0\|_{L_2} = \sqrt{\sum_{i=1}^{N_E} |T_i| \|\mathbf{u}_i - \mathbf{u}_{0,i}\|^2}. \quad (13)$$

The first one tells us if the value assumed by the variable w adjoint to the system coincides with the initial value, and the second quantity is an indicator of the effects of w on the entire system, in particular on the velocity. This choice is moreover justified by the fact that our tests are based on stationary solutions so the initial values coincide also with the exact ones.

In Figure 1 we show the values of the quantities in (13) for the test case (1) at different times. Even if the angular momentum is perfectly maintained, the velocity cannot enjoy any positive effects of including w in the system. Therefore, in Section 5 we propose a *coupled* formulation in such a way that the behavior of w and \mathbf{u} are linked together. Before presenting the second approach which couples strongly the angular momentum and the rest of the variables, we describe the test cases that will be used to analyze our methods.

Table 2: In this table we report the error in L_1 norm between the total angular momentum at the beginning of the simulation and after different times. The errors refer to three different test cases: *test 1* refers to the solid body rotation described in (1), in *test 2* the isentropic vortex of (14) is taken into account, and finally, in the third one we refer to the four vortices test case described in (15). The results show clearly the exact conservation of the angular momentum obtained with the master-slave approach both with order 1 and 2.

	test 1		test 2		test 3	
time	order 1	order 2	order 1	order 2	order 1	order 2
1	2.6E-16	1.6E-16	9.5E-14	7.3E-14	5.5E-16	7.3E-16
5	1.0E-15	8.2E-16	1.5E-14	6.7E-14	1.6E-15	1.1E-15
10	2.1E-15	1.7E-15	3.6E-15	7.9E-14	1.1E-14	7.2E-16
20	3.7E-15	3.2E-15	1.0E-13	8.9E-14	2.1E-14	1.2E-16

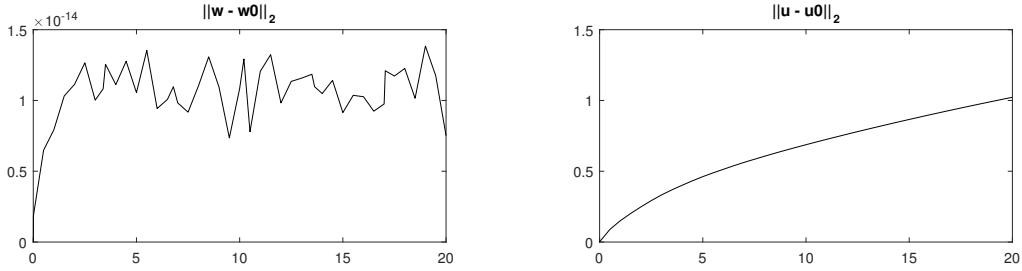


Figure 1: We consider the solid body rotation described in (1) and the master-slave formulation. We have used order one and a mesh of 1600 elements. On the left we show that the L_2 norm of the angular momentum remains stable for long times during the computation. However the L_2 norm of the velocity is rapidly dissipated and so the error grows. This means that with this formulation the velocity cannot enjoy any positive effects of including w in the system.

Isentropic vortices tests for Master-Slave

We consider a single isentropic vortex over a ring centered in the origin with radius $r \in [1, 2]$. The initial stationary condition is given by

$$\rho(r) = \left[1 - \frac{(\gamma - 1)\beta^2}{8\gamma\pi^2} e^{(1-r^2)} \right]^{\frac{1}{\gamma-1}}, \quad \mathbf{u}(r) = \frac{\beta}{2\pi} e^{\left(\frac{1-r^2}{2}\right)} (-y, x), \quad p(r) = \rho(r)^\gamma, \quad w = \mathbf{u} \wedge \mathbf{x}, \quad (14)$$

with $r = \|\mathbf{x}\|$, $\beta = 5$, $\gamma = 7/5$. See Figure 2 for the density and w profiles. In this case the center of rotation is obviously defined and coincides with the origin. A more complex example consists in considering four isentropic vortices centered respectively in $C_1 = (2.5, 2.5)$, $C_2 = (-2.5, 2.5)$, $C_3 = (-2.5, -2.5)$, $C_4 = (2.5, -2.5)$. The computational domain is a square $[-5, 5] \times [5, 5]$. The initial stationary condition is given by (14) with in particular

$$r = \begin{cases} \|\mathbf{x} - C_1\| & \text{if } x \geq 0, \text{ and } y \geq 0 \\ \|\mathbf{x} - C_2\| & \text{if } x < 0, \text{ and } y \geq 0 \\ \|\mathbf{x} - C_3\| & \text{if } x < 0, \text{ and } y < 0 \\ \|\mathbf{x} - C_4\| & \text{if } x \geq 0, \text{ and } y < 0 \end{cases}, \quad \text{and } \mathbf{u} = \begin{cases} \frac{\beta}{2\pi} e^{\left(\frac{1-r^2}{2}\right)} (-y, x), & \text{if } xy \geq 0 \\ \frac{\beta}{2\pi} e^{\left(\frac{1-r^2}{2}\right)} (y, -x), & \text{if } xy < 0. \end{cases} \quad (15)$$

See Figure 3 for the density and w profiles.

For all test problems presented in this article, unless otherwise specified, the reflective wall boundary conditions are implemented by assigning a state at the wall boundary which solves the inverse Riemann problem at the element interface such that the normal velocity $\mathbf{u} \cdot \mathbf{n}$ vanishes at the interface. A first order version of the code is employed in order to compare the three different approaches, in such a way to avoid the effects of reconstruction procedures and boundary conditions in the analysis. Finally, test (1) and (14) are run with a mesh of 1600 elements, whereas for (15) we use a mesh of 6400 elements.

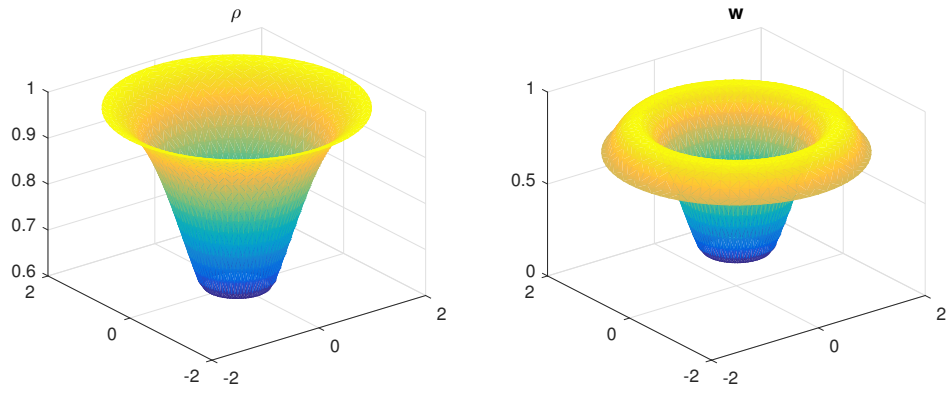


Figure 2: Density (left) and angular momentum (right) profiles for the single isentropic vortex stationary solution (14).

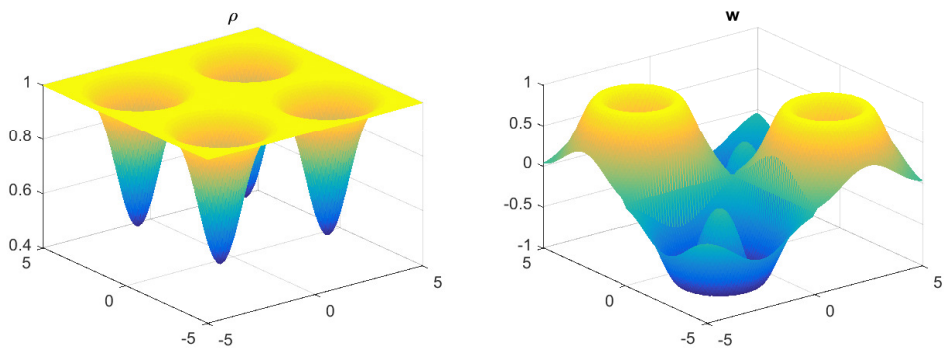


Figure 3: Density (left) and angular momentum (right) profiles for the four isentropic vortices stationary solution (15).

5. Global-coupling

In order to exploit the angular momentum preservation, we propose a coupled approach which we call *global-coupling*, referring with the term *global* to a fixed global center of rotation and in opposition to the *local-coupling* approach which will be proposed in Section 7. The global-coupling is obtained by rewriting the Euler system as follows

$$\begin{cases} \partial_t \rho + \nabla \cdot (\rho \mathbf{v}) = 0, \\ \partial_t (\rho \mathbf{u}) + \nabla \cdot (\rho \mathbf{u} \otimes \mathbf{v}) + \nabla p = \mathbf{0}, \\ \partial_t (\rho e) + \nabla \cdot (\rho \mathbf{v} e + p \mathbf{v}) = 0, \\ \partial_t (\rho w) + \nabla \cdot (\rho \mathbf{v} w) + \nabla \wedge (p(\mathbf{x} - \mathbf{x}_c)) = 0, \end{cases} \quad (16)$$

where

$$\begin{aligned} \mathbf{v} &= \mathbf{v}_r + \mathbf{v}_\theta, \quad \mathbf{v}_r = \frac{1}{r^2} \langle \mathbf{u}, (\mathbf{x} - \mathbf{x}_c) \rangle (\mathbf{x} - \mathbf{x}_c), \quad \mathbf{v}_\theta = -\frac{1}{r^2} w (\mathbf{x} - \mathbf{x}_c)^\perp, \\ r \mathbf{e}_r &= \mathbf{x} - \mathbf{x}_c, \quad r = \|\mathbf{x} - \mathbf{x}_c\|, \quad \mathbf{e}_\theta = \mathbf{e}_r^\perp, \\ e &= \epsilon + \frac{1}{2} \|\mathbf{v}_r\|^2 + \frac{1}{2r^2} w^2, \\ p &= (\gamma - 1) \left(\rho e - \frac{1}{2} \rho \left(\|\mathbf{v}_r\|^2 + \frac{1}{r^2} w^2 \right) \right). \end{aligned} \quad (17)$$

The system remains hyperbolic with an adjoint eigenvalue equal to u_n . Moreover we propose to compute the eigenvalues using \mathbf{v} instead of \mathbf{u} . Obviously, on the continuous level, one has $\mathbf{v} = \mathbf{u}$.

This formulation is obtained by noticing that, chosen a center of rotation and an orthonormal basis $(\mathbf{e}_r, \mathbf{e}_\theta)$, the velocity can be rewritten as the sum of the two components along this basis: we call \mathbf{v} the velocity when written in this way. In particular if \mathbf{u} is a radial field and \mathbf{e}_r lies along the radial direction then \mathbf{v}_r is null, which is easy to maintain even at numerical level, since classically $\|\mathbf{u}\|_{L_2}$ rapidly dissipates. Hence, the correctness of \mathbf{v} strictly depends on the preservation of w . Therefore, being able to conserve w , the expected results of employing this formulation are the following:

- a) The error on \mathbf{v} , computed *a posteriori* using (17), should be less than the error on \mathbf{u} , for this reason we introduce another indicator to measure the precision of the results

$$\|\mathbf{v} - \mathbf{v}_0\|_{L_2} = \sqrt{\sum_{i=1}^{N_E} |T_i| \|\mathbf{v}_i - \mathbf{v}_{0,i}\|^2}, \quad \text{with } \mathbf{v}_0 = \mathbf{u}_0.$$

- b) The use of \mathbf{v} , instead of \mathbf{u} , in (16) should reduce the error even on $\|\mathbf{u} - \mathbf{u}_0\|_{L_2}$ with respect to the master-slave approach.

On the other side the application of (16) is not trivial. First, appropriate boundary conditions should be defined for \mathbf{v} , w and \mathbf{x} and moreover the center of rotation should be known. As previously, the numerical method is built using our general solver by defining

$$\mathbf{Q} := \begin{pmatrix} \rho \\ \rho \mathbf{u} \\ \rho e \\ \rho w \end{pmatrix} \quad \text{and} \quad \mathbf{F}(\mathbf{Q}, \mathbf{x}) := \begin{pmatrix} \rho \mathbf{v} \\ \rho \mathbf{u} \otimes \mathbf{v} + I p \\ \rho \mathbf{v} e + p \mathbf{v} \\ \rho \mathbf{v} w + p(\mathbf{x} - \mathbf{x}_c)^\perp \end{pmatrix}$$

in (8).

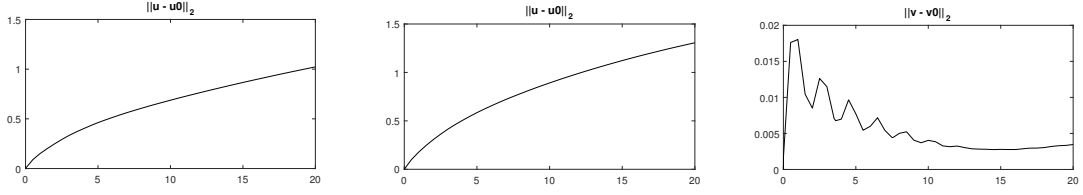


Figure 4: Consider the solid body rotation (1) and the global-coupling with standard reflective boundary conditions. In the middle we report the $\|\mathbf{u} - \mathbf{u}_0\|_{L_2}$ obtained with the global-coupling where we cannot appreciate an improving with respect to the master-slave approach (left). But instead the $\|\mathbf{v} - \mathbf{v}_0\|_{L_2}$ (right) is greatly reduced with respect to $\|\mathbf{u} - \mathbf{u}_0\|_{L_2}$.

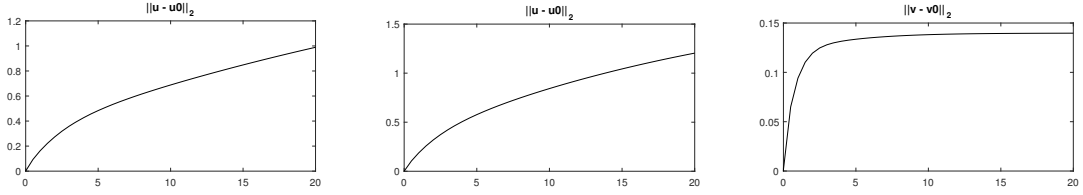


Figure 5: Consider the isotropic vortex in (14) and the global-coupling with standard reflective boundary conditions. In the middle we report the $\|\mathbf{u} - \mathbf{u}_0\|_{L_2}$ obtained with the global-coupling where we cannot appreciate an improving with respect to the master-slave approach (left). But instead the $\|\mathbf{v} - \mathbf{v}_0\|_{L_2}$ (right) is greatly reduced with respect to $\|\mathbf{u} - \mathbf{u}_0\|_{L_2}$.

Numerical results for Global-Coupling

We have applied the global-coupling to the test case (1) and to (14). In these two cases the center of rotation is known and coincides with the origin. However the treatment of boundary condition is complex. Consider a boundary element j and call i its *phantom* neighbor. An easy definition consists in considering again the reflective boundary condition and moreover to set $w_i = w_j$, $\mathbf{x}_i = \mathbf{x}_j$, and finally recovering \mathbf{v} through (17). This setting guarantees the conservation of $\|w\|_{L_1}$. Also $\|\mathbf{v} - \mathbf{v}_0\|_{L_2}$ is significantly reduced with respect to $\|\mathbf{u} - \mathbf{u}_0\|_{L_2}$. Unfortunately, no positive effects can be registered on $\|\mathbf{u} - \mathbf{u}_0\|_{L_2}$ with respect to the master-slave approach whose error is actually slightly increased. Refer to Figure 4 and 5 for the numerical results.

Another possible choice for the boundary condition consists in imposing the exact solution in the phantom element i , setting in particular \mathbf{x}_i equal to the barycenter of i . Strictly speaking we lose the conservation, but only because there is an exchange with the outside. With this choice the performance on $\|\mathbf{u} - \mathbf{u}_0\|_{L_2}$ is highly increased and at the same time $\|\mathbf{v} - \mathbf{v}_0\|_{L_2}$ grows slowly. Refer to Figure 6 and 7 for the numerical results.

This two test cases witness the potential of this formulation despite some intrinsic defects. For example, trying to apply the same scheme to the four vortices test case (15) would not improve the results, since the center of rotation, even if it is known, is not unique. With this motivation we propose the local-coupling approach where multiple centers of rotation can be considered at the same time. At first, we propose a way to detect locally the center of rotation in the following paragraph.

6. Center-Detector

Let us consider a velocity field $\mathbf{u}(\mathbf{x})$ whose value is locally given at the barycenter of each control volume $T_i \in \mathcal{T}_\Omega$ at any time step n . It can be described by the following relation

$$\mathbf{u}(\mathbf{x}) = \omega(r)(\mathbf{x} - \mathbf{x}_c)^\perp + \varphi(r)(\mathbf{x} - \mathbf{x}_c), \quad (18)$$

where \mathbf{x}_c is the center of rotation of the field, r is the distance from the center, $\omega(r)$ represents the angular velocity and $\varphi(r)$ the expansion coefficient.

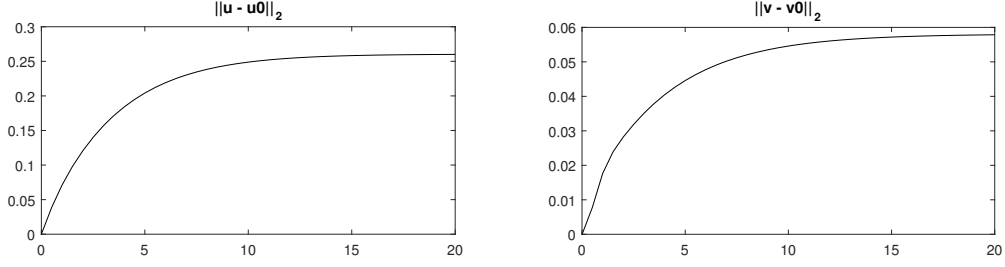


Figure 6: Consider the solid body rotation (1) and the global-coupling with the boundary conditions that exploit the exact solution. We first notice the great improving on $\|\mathbf{u} - \mathbf{u}_0\|_{L_2}$ and as counterpart only a small worsening on $\|\mathbf{v} - \mathbf{v}_0\|_{L_2}$.

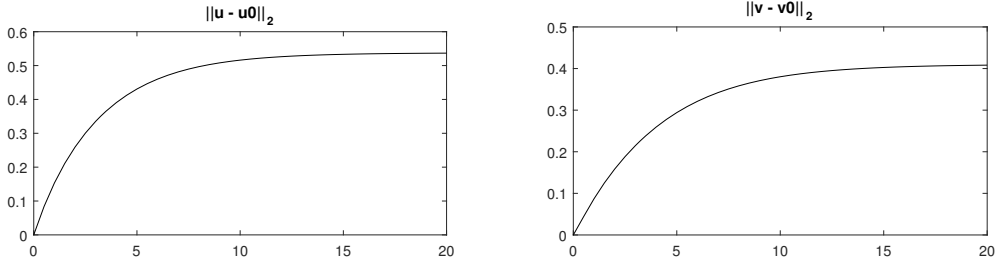


Figure 7: Consider the isentropic vortex in (14) and the global-coupling with the boundary conditions that exploit the exact solution. We first notice the great improving on $\|\mathbf{u} - \mathbf{u}_0\|_{L_2}$ and as counterpart only a small worsening on $\|\mathbf{v} - \mathbf{v}_0\|_{L_2}$.

The aim of this section is to propose a method able to reconstruct the center \mathbf{x}_c and the values of $\omega(r)$ and $\varphi(r)$, given local information about the velocity field $\mathbf{u}(\mathbf{x})$ and a radial pressure field $p = p(r)$. To fix the notation, let us consider an element T_j and its neighbors: let $\mathcal{L}(T_j)$ the set of neighbors of T_j that shares with T_j an edge, and $\mathcal{V}(T_j)$ the set of neighbors of T_j that shares with T_j a vertex. The barycenter of an element T_j is denoted by \mathbf{x}_j . All the quantities evaluated at the midpoint between two elements T_j and T_k will be denoted by a star, namely $\mathbf{x}_{j,k}^*$, $\mathbf{u}_{j,k}^*$, $r_{j,k}^*$, and for the sake of simplicity by \mathbf{x}^* , \mathbf{u}^* , r^* when there is no confusion. Refer to Figure 8 for the notation. The core of the procedure is given by the following proposition.

Proposition 6.1. *Let*

$$\varphi_{j,k}^* = \frac{\langle \mathbf{u}_j - \mathbf{u}_{j,k}^*, \mathbf{x}_j - \mathbf{x}_{j,k}^* \rangle}{\|\mathbf{x}_j - \mathbf{x}_{j,k}^*\|^2}, \quad \omega_{j,k}^* = \frac{\langle \mathbf{u}_j - \mathbf{u}_{j,k}^*, (\mathbf{x}_j - \mathbf{x}_{j,k}^*)^\perp \rangle}{\|\mathbf{x}_j - \mathbf{x}_{j,k}^*\|^2}.$$

be a local approximation of the angular velocity and of the expansion factor valid in a neighborhood of element T_j and its neighbor $T_k \in \mathcal{V}(T_j)$. Then the following first order approximations hold

$$\omega_{j,k}^* = \omega(r_j) + \omega'(r_j) r^* \left\langle \frac{\mathbf{x}^* - \mathbf{x}_c}{r^*}, \frac{\mathbf{x}_j - \mathbf{x}_k}{\|\mathbf{x}_j - \mathbf{x}_k\|} \right\rangle^2 + O(h), \quad (19)$$

$$\varphi_{j,k}^* = \varphi(r_j) + \varphi'(r_j) r^* \left\langle \frac{\mathbf{x}^* - \mathbf{x}_c}{r^*}, \frac{\mathbf{x}_j - \mathbf{x}_k}{\|\mathbf{x}_j - \mathbf{x}_k\|} \right\rangle^2 + O(h), \quad (20)$$

where h is the characteristic dimension of the elements.

Proof. We present here the proof of (19), the proof of (20) can be obtained following the same procedure.

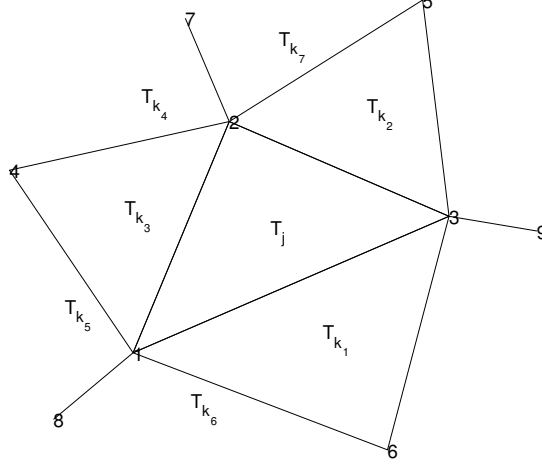


Figure 8: The element T_j and its neighbors T_{k_i} $i = 1, 2, \dots, 7$, i.e. $T_{k_1}, T_{k_2}, \dots, T_{k_7} \in \mathcal{L}(T_j)$.

From (18) the following equalities can be deduced

$$\begin{aligned}
\langle \mathbf{u}_j - \mathbf{u}^*, (\mathbf{x}_j - \mathbf{x}^*)^\perp \rangle &= \langle \omega(r_j) (\mathbf{x}_j - \mathbf{x}_c)^\perp - \omega(r^*) (\mathbf{x}^* - \mathbf{x}_c)^\perp, (\mathbf{x}_j - \mathbf{x}^*)^\perp \rangle \\
&= \langle \omega(r_j) (\mathbf{x}_j - \mathbf{x}^*)^\perp + (\omega(r_j) - \omega(r^*)) (\mathbf{x}^* - \mathbf{x}_c)^\perp, (\mathbf{x}_j - \mathbf{x}^*)^\perp \rangle \\
&= \omega(r_j) \|\mathbf{x}_j - \mathbf{x}^*\|_2 + (\omega(r_j) - \omega(r^*)) \langle \mathbf{x}^* - \mathbf{x}_c, \mathbf{x}_j - \mathbf{x}^* \rangle \\
&= \left(\omega(r_j) + \frac{\omega(r_j) - \omega(r^*)}{\|\mathbf{x}_j - \mathbf{x}^*\|_2^2} r^* \left\langle \frac{\mathbf{x}^* - \mathbf{x}_c}{r^*}, \mathbf{x}_j - \mathbf{x}^* \right\rangle \right) \|\mathbf{x}_j - \mathbf{x}^*\|_2^2.
\end{aligned} \tag{21}$$

By introducing a Taylor approximation we have that

$$\omega(r_j) - \omega(r^*) = \omega'(r_j) \left\langle \frac{\mathbf{x}^* - \mathbf{x}_c}{r^*}, \mathbf{x}_j - \mathbf{x}^* \right\rangle + O(h^2),$$

and so by substituting this last expression in (21) we finally obtain

$$\langle \mathbf{u}_j - \mathbf{u}^*, (\mathbf{x}_j - \mathbf{x}^*)^\perp \rangle = \left(\omega(r_j) + \omega'(r_j) r^* \left\langle \frac{\mathbf{x}^* - \mathbf{x}_c}{r^*}, \frac{\mathbf{x}_j - \mathbf{x}^*}{\|\mathbf{x}_j - \mathbf{x}^*\|} \right\rangle \right) \|\mathbf{x}_j - \mathbf{x}^*\|_2^2 + O(h^3), \tag{22}$$

and dividing the two members by $\|\mathbf{x}_j - \mathbf{x}^*\|_2^2$ we easily recover (19). \square

The quantity

$$\left\langle \frac{\mathbf{x}^* - \mathbf{x}_c}{r^*}, \frac{\mathbf{x}_j - \mathbf{x}_k}{\|\mathbf{x}_j - \mathbf{x}_k\|} \right\rangle \tag{23}$$

can be obtained without explicitly knowing the center \mathbf{x}_c but exploiting the radial pressure field, characterizing any flux subject to a rotation or an expansion.

Proposition 6.2. Let $p = p(r)$ be a radial pressure field then

$$p_j - p^* = \frac{p'(r^*)}{r^*} \left\langle \mathbf{x}^* - \mathbf{x}_c, \frac{\mathbf{x}_j - \mathbf{x}_k}{\|\mathbf{x}_j - \mathbf{x}_k\|} \right\rangle + \mathcal{O}(h^2), \quad (24)$$

where $p_j = p(\mathbf{x}_j)$ and $p^* = p(\mathbf{x}_{jk}^*)$, with T_k a neighbor of T_j .

Proof. The relation can be easily obtained as a Taylor expansion of p which has been supposed to depend only on r . \square

Equation (24) can be rewritten as

$$p_j - p^* = \lambda \left\langle \frac{\mathbf{x}^* - \mathbf{x}_c}{r^*}, \frac{\mathbf{x}_j - \mathbf{x}_k}{\|\mathbf{x}_j - \mathbf{x}_k\|} \right\rangle + \mathcal{O}(h^2), \quad (25)$$

with

$$\lambda = \|\mathbf{x}^* - \mathbf{x}_c\| \frac{p'(r^*)}{r^*}.$$

To simplify the notation, we remark that the two vectors in (23) and (24) are unit vectors, hence we call μ the angle between the center of rotation \mathbf{x}_c and \mathbf{x}^* , $\alpha = \cos \mu$, $\beta = \sin \mu$, and θ_k the angle between \mathbf{x}_j and \mathbf{x}_k . Now in order to obtain (23) for the element T_j by exploiting (25) we propose to find α and β such that minimize

$$\sum_{k \in \mathcal{L}(T_j)} \left| \lambda (\alpha \cos \theta_k + \beta \sin \theta_k) - \xi_k \right|, \quad \text{with} \quad \xi_k = \frac{p_j - p_k}{x_j - x_k}. \quad (26)$$

Then, the two unknowns $\omega(r_j)$ and $\omega'(r_j)$ in (19) can be recovered by exploiting the values of $\omega_{j,k}^*$ obtained from all the neighbors of T_j and by another minimization procedure. So, finally we have to solve

$$\begin{aligned} \omega(r_j), \omega'(r_j) &= \arg \min_{z_1, z_2} \sum_{k \in \mathcal{V}(T_j)} \left| z_1 + z_2 \left\langle \frac{\mathbf{x}_{j,k}^* - \mathbf{x}_c}{r_{j,k}^*}, \frac{\mathbf{x}_j - \mathbf{x}_k}{\|\mathbf{x}_j - \mathbf{x}_k\|} \right\rangle - \omega_{j,k}^* \right|^2 \\ &= \arg \min_{z_1, z_2} \sum_{k \in \mathcal{V}(T_j)} \left| z_1 + z_2 \left\langle \begin{bmatrix} \cos \mu \\ \sin \mu \end{bmatrix}, \begin{bmatrix} \cos \theta_k \\ \sin \theta_k \end{bmatrix} \right\rangle - \omega_{j,k}^* \right|^2 \\ &= \arg \min_{z_1, z_2} \sum_{k \in \mathcal{V}(T_j)} \left| z_1 + z_2 (\cos \mu \cos \theta_k + \sin \mu \sin \theta_k) - \omega_{j,k}^* \right|^2 \\ &= \arg \min_{z_1, z_2} \sum_{k \in \mathcal{V}(T_j)} \left| z_1 + z_2 \cos^2(\mu - \theta_k) - \omega_{j,k}^* \right|^2. \end{aligned} \quad (27)$$

Proposition 6.3. The uniqueness of the least square solution of (27) is guaranteed if only if the number of neighbors $T_k \in \mathcal{V}(T_j)$ with different θ_k is greater or equal than 5.

Proof. Relation (27) can be rewritten as

$$\omega(r_j), \omega'(r_j) = \arg \min_{z \in \mathcal{R}^{(2)}} \|Az - b\|_2$$

with

$$A = \begin{bmatrix} 1 & \cos^2(\mu - \theta_{k_1}) \\ 1 & \cos^2(\mu - \theta_{k_2}) \\ \vdots & \vdots \\ 1 & \cos^2(\mu - \theta_{k_m}) \end{bmatrix}, \quad z = \begin{bmatrix} z_1 \\ z_2 \end{bmatrix}, \quad b = \begin{bmatrix} \omega_{k_1}^* \\ \omega_{k_2}^* \\ \vdots \\ \omega_{k_m}^* \end{bmatrix}, \quad m = \#\mathcal{V}(T_j), \quad (28)$$

which has a unique solution if and only if $\text{rank}(A)$ is maximal, *i.e.* it is equal to two. Thus, to ensure the uniqueness, we need that at least two elements T_{k_i} and $T_{k_\ell} \in \mathcal{V}(T_j)$ are such that

$$\cos^2(\mu - \theta_{k_i}) \neq \cos^2(\mu - \theta_{k_\ell}),$$

which implies

$$\mu - \theta_{k_i} \neq \begin{cases} \pm(\mu - \theta_{k_\ell}) \\ \pm(\mu - \theta_{k_\ell}) + \pi \end{cases} \rightarrow \theta_{k_i} \neq \begin{cases} \theta_{k_\ell} \\ \theta_{k_\ell} + \pi \\ 2\mu - \theta_{k_\ell} \\ 2\mu - \theta_{k_\ell} + \pi \end{cases}. \quad (29)$$

It is clear that if $\#\mathcal{V}(T_j) \leq 4$ the angles θ_k could be exactly linked by the relations in (29). Then we need at least 5 neighbors along 5 different directions to ensure that $\text{rank}(A) = 2$. \square

Remark 6.4. *The condition given by Proposition 6.3 is in general not restrictive and always verified by any Delaunay triangulation, any structured grid. However, this tells us that the elements in $\mathcal{L}(T_j)$ are not enough to ensure the uniqueness of the solution, and so we really need to consider the set of all the neighbors $\mathcal{V}(T_j)$.*

Let us resume the fundamental steps of the algorithm: first one compute α and β through (26), then it is possible to recover $\omega(r_j)$, $\omega'(r_j)$ with (27) and finally the center \mathbf{x}_c can be obtained through (18), (19) and (20).

7. Local-coupling

As already noticed, we are interested in studying problems where the center of rotation could be unknown or there could be more than a center, so we propose a second coupled approach, that we will call *local-coupling*. The advantage of such a formulation is the possibility of defining a different center of rotation for each element of the mesh. In this way we can treat both problems with multiple *known* rotation centers and even situations for which the center is *a priori* unknown but only approximated from each element, and hence affected by numerical errors. In the later case, we shall use the local center-detector proposed in the previous section.

The difference with respect to the previous case lies in the flux computation which is done at a local level. We propose to rewrite Euler system as follows

$$\begin{cases} \partial_t \rho + \nabla \cdot (\rho \mathbf{v}^*) = 0, \\ \partial_t (\rho \mathbf{u}) + \nabla \cdot (\rho \mathbf{u} \otimes \mathbf{v}^*) + \nabla p = \mathbf{0}, \\ \partial_t (\rho e) + \nabla \cdot (\rho \mathbf{v}^* e + p \mathbf{v}^*) = 0, \\ \partial_t (\rho w) + \nabla \cdot (\rho \mathbf{v}^* w) + \nabla \wedge (p(\mathbf{x} - \mathbf{x}^*)) = 0, \end{cases} \quad (30)$$

where

$$\begin{aligned} w &= \mathbf{u} \wedge \mathbf{x}, & w^* &= w - \mathbf{u} \wedge \mathbf{x}^* \\ \mathbf{e}^* &= \frac{\mathbf{x} - \mathbf{x}^*}{r^*}, & r^* &= \|\mathbf{x} - \mathbf{x}^*\|, \\ \mathbf{v}^* &= (\mathbf{u}, \mathbf{e}^*) \mathbf{e}^* - \frac{w^*}{r^*} \mathbf{e}^{*\perp}. \end{aligned} \quad (31)$$

\mathbf{x}^* is the local center of rotation. In this later case, the numerical method is defined by writing

$$\mathbf{Q} := \begin{pmatrix} \rho \\ \rho \mathbf{u} \\ \rho e \\ \rho w \end{pmatrix} \quad \text{and} \quad \mathbf{F}(\mathbf{Q}, \mathbf{x}) := \begin{pmatrix} \rho \mathbf{v}^* \\ \rho \mathbf{u} \otimes \mathbf{v}^* + Ip \\ \rho \mathbf{v}^* e + p \mathbf{v}^* \\ \rho \mathbf{v}^* w + p(\mathbf{x} - \mathbf{x}^*)^\perp \end{pmatrix}$$

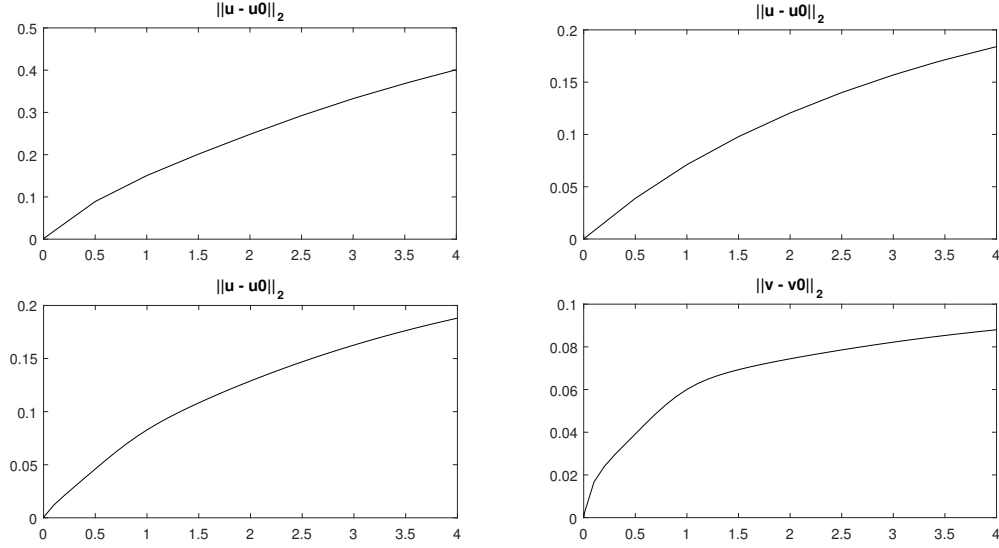


Figure 9: Consider the test case (1). Top left master-slave approach. Top right global-coupling. Bottom local-coupling with center-detector. This example shows that the local-coupling, which employs only an approximation of the center, gives results similar to the global-coupling procedure that makes use of the exact center.

in (8). Notice that if \mathbf{x}^* coincides with a unique rotation center the local-coupling method coincide with the global one.

In practical applications, \mathbf{x}^* is defined on the edges of the mesh (to compute the numerical fluxes). Logically \mathbf{x}^* is different at any edge of the mesh. Another possible choice, when computing the flux between the elements j and k through the edge ℓ_{jk} , consists in taking \mathbf{x}^* equal to the midpoint of ℓ_{jk} . With this choice the method is stable, but not significant improvements can be achieved on $\|\mathbf{u} - \mathbf{u}_0\|_{L_2}$.

Numerical results for Local-Coupling

We can test the algorithm on our test (1). Our procedure results to be quite accurate in computing the center especially when the data (*i.e.* pressure and velocity fields) are well discretized. Moreover we can couple our detector with the local-coupling method. Let us call $\bar{\mathbf{x}}_{\mathbf{c},j}$ the approximation of the center obtained through our procedure considering an element T_j and when computing the flux between T_j and T_i choose $\mathbf{x}^* = \bar{\mathbf{x}}_{ij}^*$ as

$$\mathbf{x}_{ij}^* = \frac{\bar{\mathbf{x}}_{\mathbf{c},i} + \bar{\mathbf{x}}_{\mathbf{c},j}}{2}.$$

In Figure 9 we compare the quantities $\|\mathbf{u} - \mathbf{u}_0\|_{L_2}$ obtained with the three methods we have proposed on the solid body rotation test case (1). This example shows that the local-coupling method, that employs only an approximation of the center, gives results similar to the global-coupling procedure that instead makes use of the exact center. Similar numerical results can be obtained by considering the isentropic vortex test case, see Figure 10.

7.1. Numerical criteria for general cases

In practical implementation, it does not make sense to consider the center detected by all the elements: because some of them could be affected by a shock in the velocity field, by an almost constant pressure, by a field which is not perfectly radial or by a mesh configuration particularly ill conditioned with respect to the angle of rotation μ .

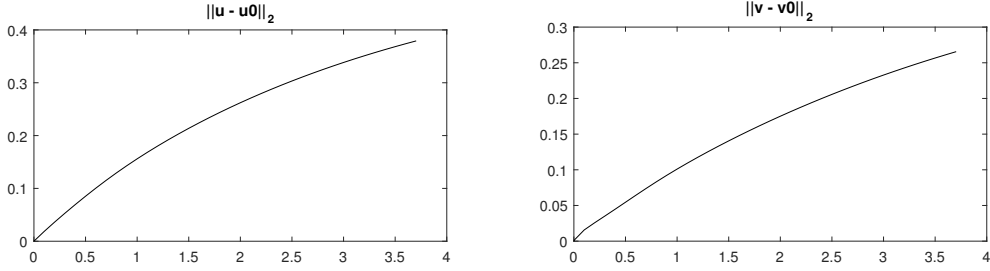


Figure 10: Consider the isentropic vortex in (14) and the local-coupling with center-detector. Even on this example this approximated procedure gives us a reduction in the velocity dissipation.

For all these reasons we propose here some numerical criteria to understand when the center detected by our algorithm could be considered as a good approximation of the exact one.

First of all, we can accept a result only when the pressure field in the neighborhood of the element has really a radial shape. So we will first exclude the element across which pressure differences are too small (*i.e.* less than 10^{-8} for example). Moreover, since the detection method is first order accurate, and from (24) we know that α and β should be approximate with an error of the order of $O(h^2)$, if the minimization procedure is affected by an error greater than

$$c_1 h$$

we will exclude this elements. Indeed, we deduce from an high variation on the estimate of α and β a non radial pressure field in the neighborhood of the considered element.

The second limitation is connected with the least square procedure described in (27). Even in this case we know the expected order of accuracy in the computations of ω and ω' , which is of order of $O(h)$. We decide to exclude all the elements for which the residuum of the least square exceeds a certain value of the form of

$$c_2 h.$$

In this way we exclude the element for which matrix A in (28) is very badly conditioned.

Lastly, recover the center by exploiting (18) could be a very difficult task because it requires to inverse a matrix whose determinant is proportional to $\Lambda = \omega^2 + \varphi^2$. If Λ is too small, its inverse will be too big and the final computation is badly conditioned. For this reason we will exclude from the computation all the element for which

$$\Lambda < c_3 h.$$

While no limitations are required if the pressure and the velocity fields are radial and well approximated, in more complex test cases the choice of c_1, c_2, c_3 can be relevant and not trivial.

By considering the four vortexes test case (15) we have verified that our detector (without the application of the previous criteria) fails in all the elements where the velocity field is too small to detect a radial field, in the elements too close to the rotation center or in the diagonal direction where the mesh configuration is particularly ill conditioned. So in Table 3 we report the results obtained by applying the numerical criteria described above: by eliminating the elements which are not suited for our detector the algorithm maintains a good precision in the determination of the center.

However its coupling with the local method does not give an improvement on the computation of the velocities: indeed for all the elements from which the center cannot be computed the choice of \mathbf{x}^* is not clear and even the boundary conditions for \mathbf{x}^* and w^* need a more sophisticated investigation. In particular choosing \mathbf{x}^* equal to the midpoint when the center is not known does not increase the quality of the results with respect to not considering w .

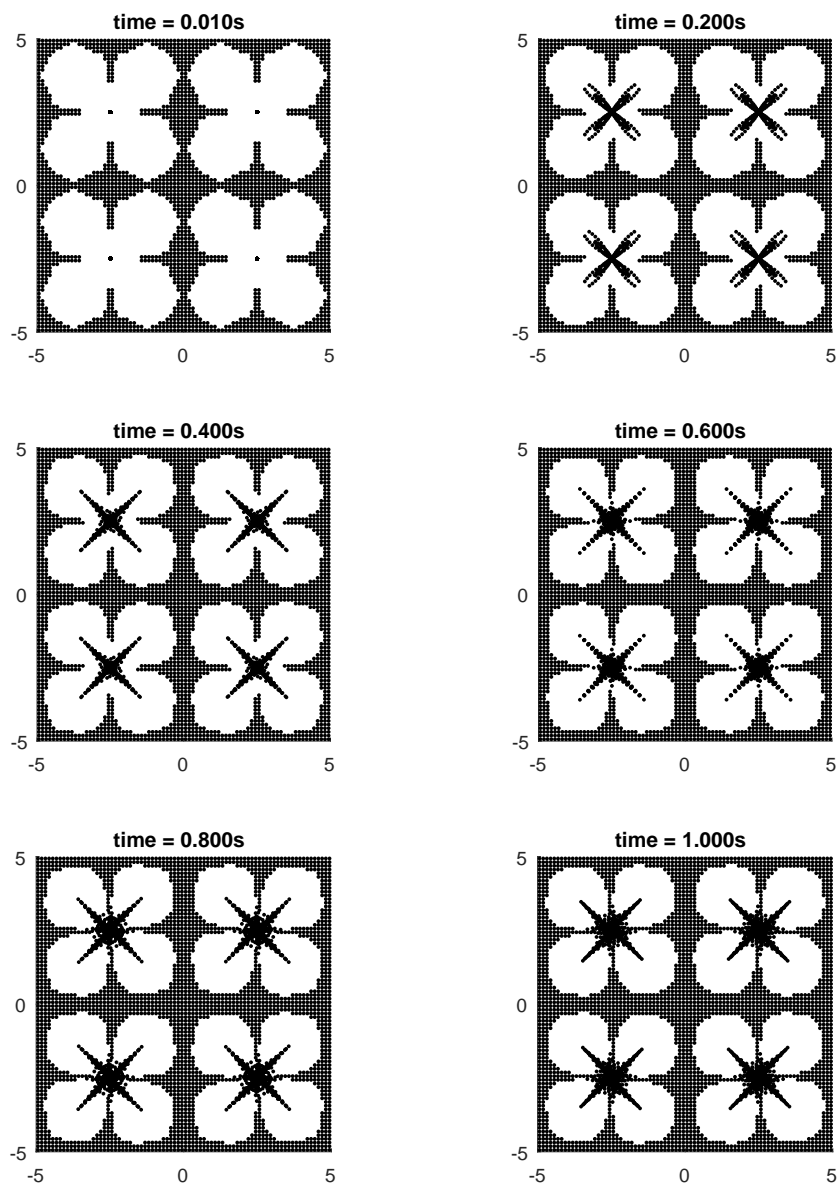


Figure 11: Four vortices test case (15). The black points represent the barycenter of the elements for which our center-detector fails. The white areas show the location of the elements for which our detector computes the center with a good precision at different times.

Table 3: Four vortexes test case (15). We have applied our detector with the numerical criteria described in 7.1 choosing in particular $c_1 = 6$, $c_2 = 10$, $c_3 = 0.1$. In the table we report the percentage of active elements and the mean error in the computation of the center obtained with a Cartesian mesh with characteristic mesh size equal to 0.125 at two different times. By mean error we mean $\frac{\sum_{j \in \text{active elements}} \|\mathbf{x}_{c,j} - \mathbf{x}_c\|}{\# \text{ active elements}}$. The error are of the order of the mesh size, as expected.

time	active elements	error
0	37%	0.15
1.2	33%	0.18

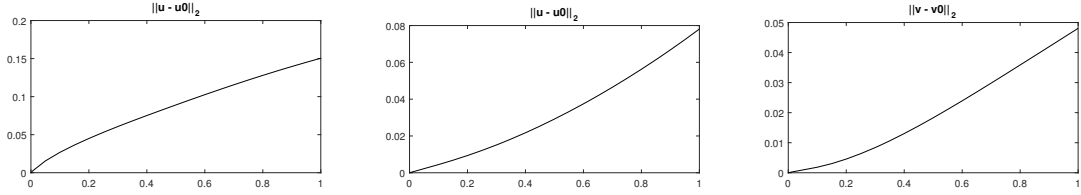


Figure 12: Consider the solid body rotation (1) with boundary condition given by the exact solution. We compare the results obtained with the master-slave approach with a zero velocity mesh (left) and the global-coupling formulation in the ALE framework (middle and right). We can notice that even in the complex situation of a moving mesh the global-coupling allows a better preservation of the velocity norm.

8. Coupling with ALE techniques

We underline that all the test cases presented up to now are run with a zero velocity mesh. The coupling with the ALE techniques is not trivial: again because of the boundary conditions of the adjoint quantities \mathbf{x} , w , \mathbf{v} but even because of the standard distortion problems of considering a moving domain. However, taking into account the test case (1) and imposing the boundary conditions through the exact solution we can see that the global formulation allows a better preservation of the velocity norm even in this context at least for small times, refer to Figure 12.

9. A Kidder problem with rotation

A solution depending on three coefficients $\bar{\rho} > 0$, $\alpha \geq 0$ and $R_0 > 0$ writes

$$\begin{cases} \rho_0(R) = \bar{\rho} \left(\frac{R^2}{R_0^2} + \alpha \right), \\ p_0(R) = \widehat{p} \left(\frac{R^2}{R_0^2} + \alpha \right)^2, \quad \widehat{p} = \frac{1}{4} \bar{\rho} \frac{R_0^2}{\tau^2} = (1 + \omega^2 \tau^2) \frac{1}{4} \bar{\rho} \frac{R_0^2}{\tau^2}. \end{cases} \quad (32)$$

The full derivation is in the Appendix A. The other initial data are $u_\theta(R) = \omega R$ and $u_r(R) = 0$. This solution is very similar to the Kidder solution for $\omega = 0$, but the pressure is premultiplied by the constant factor $1 + \omega^2 \tau^2$ to counterbalance the centrifugal force created by the angular solid body rotation.

For our test case we have chosen $R_2 = 1$, $R_1 = 0.9$, $\rho_2 = 2$ and $\rho_1 = 1$. This corresponds to a focusing time of $\tau \simeq 0.21794$ and we run the simulation until $t_f = 0.6\tau$. The initial angular velocity is $\omega = \tau^{-1}$ so that the pressure is, with respect to the classical Kidder solution, multiplied by a constant factor 2. The boundary conditions are imposed by prescribing the outer exact value of density, velocity and pressure.

In Figure 14 we report the density and the angular momentum contours of our numerical solution (obtained with the master-slave approach) compared with the analytical one.

Moreover, in Table 4 we report the errors over the density, the velocity and the angular momentum obtained both with the master-slave and the global-coupling approaches. We underline that the results obtained with the global-coupling do not improve the overall quality because in this test case the velocity field has a non null radial component: so even if the angular component is approximate through the angular

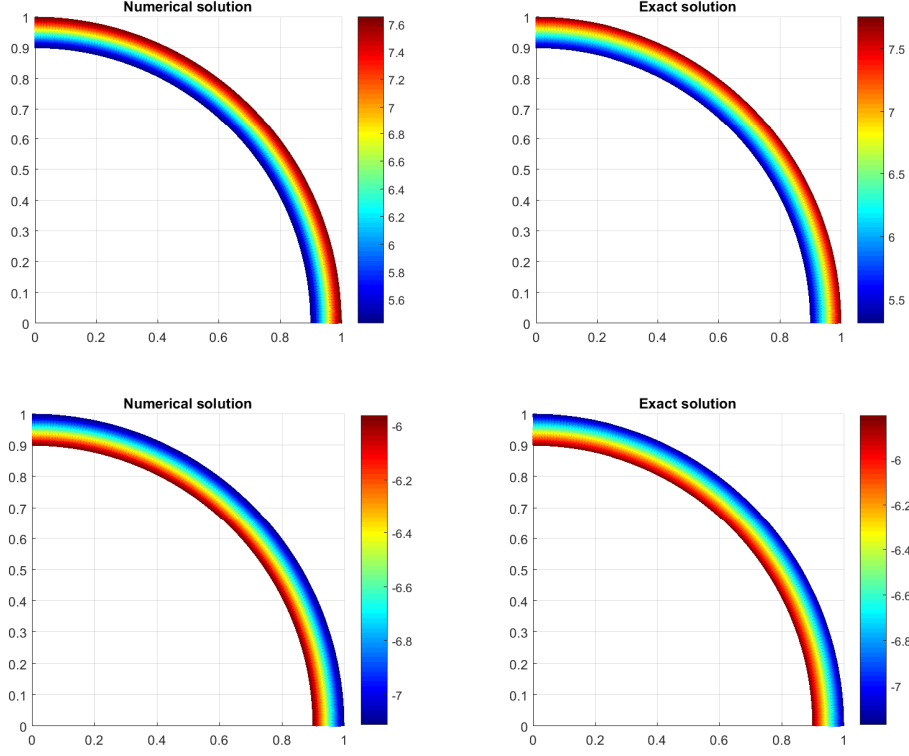


Figure 13: Kidder with rotation test case at the final time $t_f = 0.6\tau$ with an Eulerian scheme. We compare the numerical solution (left) with the analytical one (right), considering the density profile (top) and the angular momentum (bottom). The numerical results have been obtained with the first order master-slave approach and a mesh with 6280 quadrilateral elements.

momentum, no positive effects can be seen on the radial component. However this does not prevent the convergence of the method.

Finally, we have performed the same test moving the mesh with the fluid velocity. In particular the Cheng and Shu node solver [9, 15] have been employed to compute the velocity of each node of the mesh. We report our numerical results, obtained both with the master-slave and the global-coupling approaches, in Figure 14 and in Table 5.

10. Conclusion

We have presented three different approaches in order to exploit the adjoint equation for the angular momentum and increase the capabilities of our scheme. The conservation of the angular momentum is

Table 4: Kidder with rotation test case at the final time $t_f = 0.6\tau$ with zero mesh velocity. We report the L_2 norm of the error over ρ , \mathbf{u} and w with respect to the exact solution $\bar{\rho}$, $\bar{\mathbf{u}}$, \bar{w} .

mesh h	master-slave approach			global-coupling approach		
	$\ \rho - \bar{\rho}\ _{L_2}$	$\ \mathbf{u} - \bar{\mathbf{u}}\ _{L_2}$	$\ w - \bar{w}\ _{L_2}$	$\ \rho - \bar{\rho}\ _{L_2}$	$\ \mathbf{u} - \bar{\mathbf{u}}\ _{L_2}$	$\ w - \bar{w}\ _{L_2}$
2.03E-04	4.15E-2	4.82E-1	7.79E-1	6.26E-2	6.96E-1	9.48E-1
9.50E-05	2.77E-2	2.99E-1	4.97E-1	3.81E-2	4.30E-1	6.09E-1

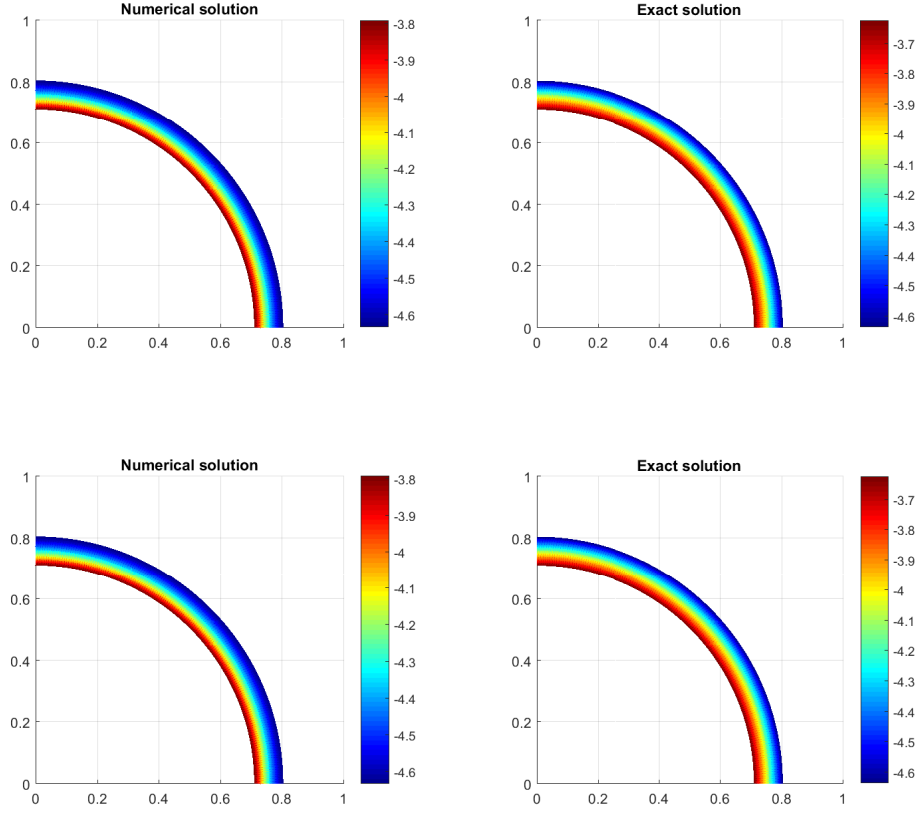


Figure 14: Kidder with rotation test case at the final time $t_f = 0.6\tau$ with the ALE scheme. We compare the numerical solution (left) with the analytical one (right), considering the density profile (top) and the angular momentum (bottom). The numerical results have been obtained with the first order master-slave approach and a mesh of 6280 quadrilateral elements.

Table 5: Kidder with rotation test case at the final time $t_f = 0.6\tau$ with the ALE code. We report the L_2 norm of the error over ρ , \mathbf{u} and w with respect to the exact solution $\bar{\rho}$, $\bar{\mathbf{u}}$, \bar{w} .

mesh	master-slave approach			global-coupling approach		
	$\ \rho - \bar{\rho}\ _{L_2}$	$\ \mathbf{u} - \bar{\mathbf{u}}\ _{L_2}$	$\ w - \bar{w}\ _{L_2}$	$\ \rho - \bar{\rho}\ _{L_2}$	$\ \mathbf{u} - \bar{\mathbf{u}}\ _{L_2}$	$\ w - \bar{w}\ _{L_2}$
2.03E-04	4.11E-2	2.18E-1	1.90E-1	3.82E-2	5.09E-1	4.27E-1
9.50E-05	2.12E-2	1.78E-1	9.63E-2	2.56E-2	3.75E-1	3.09E-1

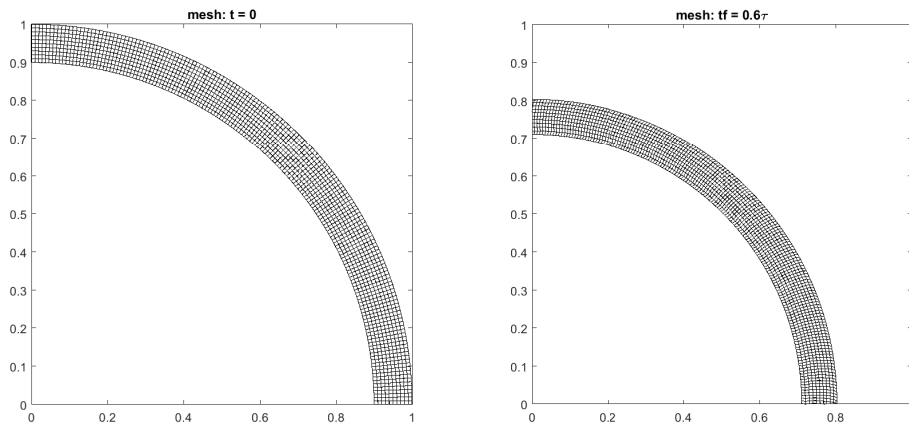


Figure 15: Initial and final mesh relative to the Kidder with rotation test case performed with the ALE code [12] on a coarse mesh, with Rusanov-type numerical flux and without nonconforming sliding lines.

guaranteed by solving the augmented system for all the presented test cases. Moreover, we have presented some test cases where the preservation of the angular momentum allows also to maintain good velocity profiles for long times, better than the one obtained with standard methods. This both when the center of rotation is known and when it is approximated.

Despite the good results obtained with simple test cases on symmetric domains this work represents only a starting point: indeed the extension to more complex situations would need further investigations. Furthermore the center-detector could be used in other contexts. In particular one may think to use it in cases with non stationary centers, or in combination with MUSCL-type second order reconstruction.

Acknowledgments

The research presented in this paper has been partially financed by the European Research Council (ERC) under the European Union's Seventh Framework Programme (FP7/2007-2013) with the research project *STiMulUs*, ERC Grant agreement no. 278267. Moreover this project has been supported by the Erasmus+ Programme of the European Union.

References

- [1] Anthony A Amsden, PJ O'rourke, and TD Butler. Kiva-ii: A computer program for chemically reactive flows with sprays. Technical report, Los Alamos National Lab., NM (USA), 1989.
- [2] T.J. Barth and D.C. Jespersen. The design and application of upwind schemes on unstructured meshes. *AIAA Paper 89-0366*, pages 1–12, 1989.
- [3] David J. Benson. Computational methods in lagrangian and eulerian hydrocodes. *Computer Methods in Applied Mechanics and Engineering*, 99(2):235 – 394, 1992.
- [4] Markus Berndt, Jérôme Breil, Stéphane Galera, Milan Kucharik, Pierre-Henri Maire, and Mikhail Shashkov. Two-step hybrid conservative remapping for multimaterial arbitrary lagrangian–eulerian methods. *Journal of Computational Physics*, 230(17):6664–6687, 2011.
- [5] Book and Berstein. Fluid instabilities of a uniformly imploding ablatively driven shell. *Journal of Plasma Physics*, 1980.

- [6] Walter Boscheri, Dinshaw S Balsara, and Michael Dumbser. Lagrangian ader-weno finite volume schemes on unstructured triangular meshes based on genuinely multidimensional hll riemann solvers. *Journal of Computational Physics*, 267:112–138, 2014.
- [7] Walter Boscheri and Michael Dumbser. Arbitrary-lagrangian-eulerian one-step weno finite volume schemes on unstructured triangular meshes. *Communications in Computational Physics*, 14(05):1174–1206, 2013.
- [8] Walter Boscheri, Michael Dumbser, and DS Balsara. High-order ader-weno ale schemes on unstructured triangular meshes application of several node solvers to hydrodynamics and magnetohydrodynamics. *International Journal for Numerical Methods in Fluids*, 76(10):737–778, 2014.
- [9] J. Cheng and C.W. Shu. A high order ENO conservative Lagrangian type scheme for the compressible Euler equations. *Journal of Computational Physics*, 227:1567–1596, 2007.
- [10] Bruno Després and Emmanuel Labourasse. Angular momentum preserving cell-centered lagrangian and eulerian schemes on arbitrary grids. *Journal of Computational Physics*, 290:28–54, 2015.
- [11] John K Dukowicz and Bertrand JA Meltz. Vorticity errors in multidimensional lagrangian codes. *Journal of Computational Physics*, 99(1):115–134, 1992.
- [12] Elena Gaburro, Michael Dumbser, and Manuel J Castro. Direct arbitrary-lagrangian-eulerian finite volume schemes on moving nonconforming unstructured meshes. *arXiv preprint arXiv:1602.01703*, 2016.
- [13] Stephen C Jardin. Review of implicit methods for the magnetohydrodynamic description of magnetically confined plasmas. *Journal of Computational Physics*, 231(3):822–838, 2012.
- [14] Roger Kaeppli and S Mishra. Structure preserving schemes. *ETH Zürich*, 2014.
- [15] W. Liu, J. Cheng, and C.W. Shu. High order conservative Lagrangian schemes with LaxWendroff type time discretization for the compressible Euler equations. *Journal of Computational Physics*, 228:8872–8891, 2009.
- [16] A Mignone, M Flock, M Stute, SM Kolb, and G Muscianisi. A conservative orbital advection scheme for simulations of magnetized shear flows with the pluto code. *Astronomy & Astrophysics*, 545:A152, 2012.
- [17] Abraham H Oort. Angular momentum cycle in the atmosphere-ocean-solid earth system. *Bulletin of the American Meteorological Society*, 70(10):1231–1242, 1989.
- [18] Ilias Petropoulos, Michel Costes, and Paola Cinnella. Development and analysis of high-order vorticity confinement schemes. *Computers & Fluids*, 2017.
- [19] Philip Roe and Bill Morton. Preserving vorticity in finite-volume schemes. *FINITE VOLUME FOR COMPLEX APPLICATIONS. Volum 2, Problems and Perspectives*, 2:347, 1999.
- [20] M Aaron Skinner and Eve C Ostriker. The athena astrophysical magnetohydrodynamics code in cylindrical geometry. *The Astrophysical Journal Supplement Series*, 188(1):290, 2010.
- [21] B. van Leer. Towards the ultimate conservative difference scheme II: Monotonicity and conservation combined in a second order scheme. *Journal of Computational Physics*, 14:361–370, 1974.

A. Implosion of Kidder type with rotation

The Kidder test problem is emblematic of strong implosion in stars or for inertial confinement devices. Starting from the standard Kidder problem, we show how to add a rotation to the initial condition. The derivation of the analytical solution is described using the seminal method of [5]. One starts with the Euler equations in general dimension $d \geq 1$

$$\begin{cases} D_t \rho + \rho \nabla \cdot \mathbf{v} = 0, & D_t = \partial_t + \mathbf{v} \cdot \nabla, \\ \rho D_t \mathbf{v} + \nabla p = \mathbf{0}, \\ D_t(p/\rho^\gamma) = 0. \end{cases}$$

For a flow with rotation invariance it can be recast as

$$\begin{cases} D_t \rho + \rho r^{-(d-1)} \partial_r (r^{d-1} u_r) = 0, & \mathbf{v} = u_r \mathbf{e}_r + u_\theta \mathbf{e}_\theta, \\ \rho D_t u_r + \partial_r p = F_{\text{centrifugal}}, & F_{\text{centrifugal}} = \rho u_\theta^2 / r, \\ D_t (u_\theta r) = 0, & (\text{conservation of angular momentum}) \\ D_t (p/\rho^\gamma) = 0. \end{cases}$$

The new feature with respect to the standard Kidder solution is the non zero angular velocity u_θ . One looks for a self-similar solution $r = Rf(t)$ with $u_r = D_t r = Rf'(t) = rf'(t)f(t)^{-1}$.

One gets $\rho = \rho_0(R)f(t)^{-d}$ where $\rho_0(R)$ is the density at time $t = 0$. This can be checked as follows: one has

$$D_t \rho = \partial_{tR} (\rho_0(R)f(t)^{-d}) = -\rho_0(R)df(t)^{-(d+1)}$$

and

$$\begin{aligned}\rho r^{-(d-1)}\partial_r(r^{d-1}u_r) &= \rho\partial_r u_r + \rho(d-1)r^{-1}u_r = \rho f'(t)f(t)^{-1} + \rho(d-1)f'(t)f(t)^{-1} \\ &= \rho df'(t)f(t)^{-1} = \rho_0(R)df'(t)f(t)^{-(d+1)}.\end{aligned}$$

By summation, one gets the continuity equation $D_t\rho + \rho r^{-(d-1)}\partial_r(r^{d-1}u_r) = 0$. The adiabaticity of the flow yields $p = p_0(r)(\rho/\rho_0(R))^\gamma$ that is $p = p_0(R)f(t)^{-\gamma d}$. Moreover one has the identities

$$\begin{cases} \rho D_t u_r = f(t)^{-d}\rho_0(R)Rf''(t), \\ \partial_r p = f(t)^{-1}\partial_R p = f(t)^{-(\gamma d+1)}p'_0(R), \\ \rho u_\theta^2/r = f(t)^{-(d+3)}\rho_0(R)(u_\theta)_0(R)^2/R. \end{cases}$$

The Newton equation $\rho D_t u_r + \partial_r p = \rho u_\theta^2/r$ is an identity between the above 3 terms. It yields

$$f(t)^{-d}\rho_0(R)Rf''(t) + f(t)^{-(\gamma d+1)}p'_0(R) = f(t)^{-(d+3)}\rho_0(R)(u_\theta)_0(R)^2/R. \quad (33)$$

As in [5], the solution is seek by separation of variables.

However a preliminary manipulation is necessary because the identity (33) is made with 3 contributions. We equate the power of the terms which are non differential with respect to $f(t)$ using $\gamma d + 1 = d + 3 \iff \gamma = \frac{d+2}{d} = 2$. One gets

$$\rho_0(R)Rf(t)^3 f''(t) = \rho_0(R)w_0(R)^2/R - p'_0(R).$$

A classical solution [5] by separation of variables of such an equation is $f(t) = \sqrt{1 - t^2/\tau^2}$ where $\tau > 0$ is a focalization time, so that $f(t)^3 f''(t) = -\tau^{-2}$. It remains to discuss the reduced equation

$$p'_0(R) = \rho_0(R)R\tau^{-2} + \rho_0(R)w_0(R)^2/R. \quad (34)$$

We decide for convenience of a rigid body rotation which corresponds to $w_0(R) = \omega R$ where ω is a given angular velocity. Let us define $\hat{\tau}^{-2} = \tau^{-2} + \omega^2$ so that (34) rewrites

$$p'_0(R) = \rho_0(R)R\hat{\tau}^{-2}. \quad (35)$$